Redox Biology 72 (2024) 103129

Contents lists available at ScienceDirect

Redox Biology

journal homepage: www.elsevier.com/locate/redox

Semaglutide attenuates doxorubicin-induced cardiotoxicity by ameliorating BNIP3-Mediated mitochondrial dysfunction

Xiaoping Li [a,b,1], Wenbin Luo [a,b,1], Yang Tang [a,c,1], Jiangjiao Wu [a,b,1], Junkai Zhang [a,b], Shengnan Chen [a,b], Lu Zhou [a,b], Yu Tao [a,b], Yuanjuan Tang [a,b,d], Fengxian Wang [a,b], Yu Huang [e], Pedro A. Jose [f], Li Guo [g,**], Chunyu Zeng [a,b,h,i,j,*]

[a] Department of Cardiology, Daping Hospital, Third Military Medical University (Army Medical University), Chongqing, China
[b] Key Laboratory of Geriatric Cardiovascular and Cerebrovascular Disease Research, Ministry of Education of China, Chongqing Key Laboratory for Hypertension Research, Chongqing Cardiovascular Clinical Research Center, Chongqing Institute of Cardiology, Chongqing, China
[c] College of Bioengineering, Chongqing University, Chongqing, China
[d] Department of Cardiology, The Third People's Hospital of Hospital of Chengdu, Affiliated Hospital of Southwest Jiaotong University, Chengdu, China
[e] Department of Biomedical Sciences, City University of Hong Kong, Hong Kong Special Administrative Region, China
[f] Division of Renal Diseases & Hypertension, The George Washington University School of Medicine & Health Sciences, Washington, DC, USA
[g] Endocrinology Department, The First Affiliated Hospital of the Third Military Medical University (Army Medical University), Chongqing, China
[h] State Key Laboratory of Trauma, Burns and Combined Injury, Daping Hospital, Third Military Medical University, Chongqing, China
[i] Center of Chongqing College, Chinese Academy of Sciences, University of Chinese Academy of Sciences, Chongqing, China
[j] Department of Cardiology, The First Affiliated Hospital of Kunming Medical University, Kunming, Yunnan Province, China

ARTICLE INFO

Keywords:
BNIP3
Doxorubicin-induced cardiotoxicity
Mitochondria
PI3K/AKT
Semaglutide

ABSTRACT

Aims: Doxorubicin is a powerful chemotherapeutic agent for cancer, whose use is limited due to its potential cardiotoxicity. Semaglutide (SEMA), a novel analog of glucagon-like peptide-1 (GLP-1), has received widespread attention for the treatment of diabetes. However, increasing evidence has highlighted its potential therapeutic benefits on cardiac function. Therefore, the objective of this study was to examine the efficacy of semaglutide in ameliorating doxorubicin-induced cardiotoxicity.

Methods and results: Doxorubicin-induced cardiotoxicity is an established model to study cardiac function. Cardiac function was studied by transthoracic echocardiography and invasive hemodynamic monitoring. The results showed that semaglutide significantly ameliorated doxorubicin-induced cardiac dysfunction. RNA sequencing suggested that *Bnip3* is the candidate gene that impaired the protective effect of semaglutide in doxorubicin-induced cardiotoxicity. To determine the role of BNIP3 on the effect of semaglutide in doxorubicin-induced cardiotoxicity, BNIP3 with adeno-associated virus serotype 9 (AAV9) expressing cardiac troponin T (cTnT) promoter was injected into tail vein of C57/BL6J mice to overexpress BNIP3, specifically in the heart. Overexpression of BNIP3 prevented the improvement in cardiac function caused by semaglutide. *In vitro* experiments showed that semaglutide, via PI3K/AKT pathway, reduced BNIP3 expression in the mitochondria, improving mitochondrial function.

Conclusion: Semaglutide ameliorates doxorubicin-induced mitochondrial and cardiac dysfunction via PI3K/AKT pathway, by reducing BNIP3 expression in mitochondria. The improvement in mitochondrial function reduces doxorubicin-mediated cardiac injury and improves cardiac function. Therefore, semaglutide is a potential therapy to reduce doxorubicin-induced acute cardiotoxicity.

* Corresponding author. Department of Cardiology, Daping Hospital, Third Military Medical University (Army Medical University), Chongqing, China.
** Corresponding author.
E-mail addresses: dearpeardog@126.com (L. Guo), zengchunyu@tmmu.edu.cn (C. Zeng).
[1] The first four authors contributed equally to the study.

https://doi.org/10.1016/j.redox.2024.103129
Received 12 January 2024; Received in revised form 16 March 2024; Accepted 18 March 2024
Available online 19 March 2024

1. Introduction

Doxorubicin (DOX), an anthracycline antibiotic commonly used to treat a range of cancers, including breast cancer, bladder cancer, ovarian cancer, gastric cancer, lung cancer, thyroid cancer, and advanced esophageal squamous cell carcinoma, is one of the most effective anticancer drugs available [1–5]. However, several side effects limit its therapeutic value, including cardiotoxicity, which may cause irreversible loss in cardiac function and subsequently, heart failure [6,7]. Currently, dexrazoxane is the only FDA-approved cardioprotective agent specifically indicated in patients receiving anthracycline chemotherapy. Nevertheless, it is worth noting that dexrazoxane may potentially trigger adverse effects such as bone marrow suppression, liver toxicity, and the development of secondary malignant tumors [8]. Therefore, more efficient and safer cardioprotective drugs for chemotherapy-related cardiotoxicity are needed.

Antihyperglycemic medications, such as glucagon-like peptide-1 (GLP-1) receptor agonists, have been found to improve left ventricular function in patients with acute myocardial infarction and severe systolic dysfunction [9,10]. Additionally, they improved left ventricular ejection fraction and functional status in patients with chronic heart failure [11]. While the cardioprotective effects of GLP-1 receptor agonist are well-established, their effect on doxorubicin-induced cardiotoxicity has not been well investigated. Given the role of semaglutide, one GLP-1 analog, in cardioprotection, it is plausible that semaglutide may offer protection against doxorubicin-induced cardiac dysfunction. Therefore, our present study examined the effect of semaglutide on doxorubicin-induced cardiotoxicity and investigated its underlying mechanisms.

2. Materials and methods

2.1. Animals

Six-week-old C57/BL6J mice were obtained from the laboratory animal center of Daping Hospital, Third Military Medical University (Chongqing, China). The mice were housed in and treated at the Animal Centre of Daping Hospital, where they were maintained under specific pathogen-free, environmentally controlled (temperature: 20–25 °C; humidity: 50 ± 5%) barrier conditions in individual ventilated cages and fed with sterile food and water ad libitum. Following a week of acclimatization, the mice were randomly assigned to individual groups. The mice were administered doxorubicin (i.p. 5 mg/kg; MedChemExpress, Monmouth Junction, NJ) or an equivalent volume of the vehicle (saline) once a week for 4 weeks [12]. Semaglutide (12 μg/kg; Novo Nordisk, Copenhagen, Denmark) was subcutaneously injected daily for 6 weeks as shown in Fig. S1A [13]. For the overexpression of BNIP3, the mice received a single intravenous injection of an adeno-associated serotype 9 (HBAAV2/9-cTNT-*m*-Bnip3-2 × flag-EGFP) viral vector or negative control (HBAAV2/9-cTNT-EGFP) (Hanbio Biotechnology, Shanghai, China), via the tail vein at a concentration of 5×10^{10} viral genome per mouse and studied after 4 weeks (Fig. S1B). At the end of the experiment, all mice were anesthetized with isoflurane (5%) and euthanized by cervical dislocation. The experimental procedures received ethical approval from the Institutional Animal Care and Use Committee of the Third Military Medical University (ethical approval number: AMUWEC20229024), adhering to the guidelines stated in the NIH Guide for the Care and Use of Laboratory Animals.

2.2. Echocardiography

Echocardiography was performed using a high-resolution ultrasound imaging system (Vevo 2100, Visual Sonics, Canada). Briefly, the mice were anesthetized with 1.5% isoflurane and 98.5% O_2 and placed in a supine position on a temperature-controlled heating platform to maintain a body temperature of 37 °C. The parasternal long axis plane was used to calculate the systolic function index during the M-type measurement, using the Vevo analysis software (Vevo LAB 5.5.1), taking the average of at least three consecutive heartbeats. The investigators performing these studies were blinded to the drug interventions.

2.3. Invasive hemodynamics

Isoflurane (3% for induction; 1.5% for maintenance mixed with 98.5% oxygen) was used to anesthetize the animals. The mice were placed on regulated heating pads to keep their body temperatures at 37 °C and after having their tracheas intubated were subsequently artificially ventilated, using a volume-controlled ventilator trach. The left external jugular vein was cannulated with a polyethylene catheter to provide fluids. The right carotid artery was used as the entry point for a 1.4 F micro tip pressure-conductance micro-catheter (SPR-839, Millar Instruments, Houston, TX), which was inserted past the aortic valve and into the left ventricle (LV). Following a 5-min stabilization period, the signals were continuously collected using a pressure-volume (P-V) conductance system coupled to a Power Lab 16/30 data collection system (AD Instruments, Colorado Springs, CO), at a sampling rate of 1000 samples/s. The abdominal inferior vena cava (IVC) was briefly occluded, to allow construction of variably loaded pressure-volume loops, from which LV end-systolic (ESPVR) and end-diastolic pressure-volume relations (EDPVR) were calculated [14].

2.4. Histological analysis

The heart samples were initially fixed in 4% paraformaldehyde at 4 °C for 1–2 days, followed by dehydration in ethanol. Afterwards, the samples were cleared with xylene and then embedded in paraffin. Subsequently, the samples were sliced into sections with a thickness of 4 μm. In order to assess cardiac morphology, fibrosis, and cardiac myocyte area (CSA), the tissue sections were subjected to specific staining procedures. Hematoxylin and eosin (H&E) staining (G1120, Solarbio, Beijing, China), Masson's trichrome staining (G1345, Solarbio), and wheat germ agglutinin (WGA) staining (W11261, Thermo Fisher Scientific, Waltham, MA) were utilized, following standard protocols. The sections were visualized using an Olympus SlideView VS200 microscope (Olympus, Hamburg, Germany). Quantitative analysis of the staining was conducted in a blinded manner using Image J software.

2.5. Cardiac marker enzymes measurements

BNP (HB533-Mu, Hengyuan Biological Technology, Shanghai, China), CK-MB (HB761-Mu, Hengyuan Biological Technology) and LDH (HB1402-Mu, Hengyuan Biological Technology) serum levels were measured using commercial kits. LDH release was measured using an LDH cytotoxicity assay kit (HY-K1090, MedChemExpress). All commercially available kits were used according to the manufacturer's instructions.

2.6. Oxidative stress detection and cell viability

Reactive oxygen species (ROS) production was measured *in vivo* using DHE staining [15] (S0063, Beyotime, Shanghai, China) and *in vitro* using MitoSOX Red staining [16] (HY-D1055, MedChemExpress). In brief, cryosections of fresh heart samples or on coverslips were stained with DHE (5 μmol/L) or MitoSOX Red (5 μmol/L) in the dark at 37 °C for 30 min. The stained samples were then examined under an Olympus SlideView VS200 microscope in a blinded manner. Cell viability was determined using a calcein/PI cell viability/cytotoxicity assay kit [17] (C2015 M, Beyotime). After incubation with the calcein/PI buffer for 30 min, live cells (green) and dead cells (red) were observed under an Olympus SlideView VS200 microscope.

2.7. Seahorse respirometry

Seahorse respirometry was using the Seahorse XFe24 Extracellular Flux Analyzer and Seahorse XF24 FluxPaks (Agilent Technologies, Waldbronn, Germany). To evaluate oxygen consumption rates (OCR), primary cardiomyocytes were seeded in an assay microplate at 4×10^4 cells/well in growth medium. After treatment with indicated reagents for indicated period, the culture medium was replaced with Seahorse XF DMEM buffer. The OCR was assessed at the basal level and following metabolic perturbations with 1.5 μmol/L oligomycin, 1 μmol/L FCCP (mitochondrial uncoupler), and 0.5 μmol/L rotenone, and antimycin A. Calculations were performed using the Agilent Seahorse Wave Software for Agilent Seahorse XF analyzers (Seahorse Bioscience).

2.8. TUNEL staining

TUNEL staining of heart slices used a one-step TUNEL In Situ Apoptosis Kit (E-CK-A331, Elabscience, Wuhan, China). Images were obtained using Olympus SlideView VS200 microscope.

2.9. Immunofluorescence staining

Heart sections were deparaffinized and rehydrated using a gradient elution method with xylene and ethanol. Antigen retrieval was performed by incubation in citrate antigen retrieval solution (P0081, Beyotime) at 95 °C for 20 min. The cells were fixed with 4% paraformaldehyde for 15 min at room temperature. The prepared heart sections and cells were blocked by incubation in QuickBlock™ Immunostaining Blocking Solution (P0260, Beyotime) at 37 °C for 30 min, followed by overnight incubation at 4 °C with primary antibodies against γ-H2AX (1:200, ab81299, Abcam, Cambridge, MA), cardiac troponin T (1:200, ab209813, Abcam), and BNIP3 (1:200, ab109362, Abcam). The slides were then incubated with Alexa Fluor 488™ secondary antibody (1:200, A-11008, Thermo Fisher Scientific) or Alexa-Fluor555™ secondary antibody (1:200, A-11035, Thermo Fisher Scientific) in the dark at 37 °C for 1 h. The nucleus was counterstained with DAPI (C1006, Beyotime, China). Each step was followed by washing with PBS three times for 5 min. The images were captured using laser confocal microscopy and analyzed with the Olympus Fluoview FV300 version 3C Acquisition Software. Quantitative analysis of the fluorescence intensity was conducted in a blinded manner using Image J software.

2.10. RNA-seq analysis

The hearts from C57/BL6J mice, with or without semaglutide treatment, were collected for further analysis. RNA isolation, quality control, library construction, and sequencing were carried out by Shanghai Applied Protein Technology (https://www.aptbiotech.com). The library preparations were then subjected to sequencing on an Illumina Novaseq 6000 platform. Subsequent bioinformatics analyses were performed using RStudio (Version 2022.07.2 Build 576). Differential expression analyses were conducted using DESeq2 (R packages v1.38.1) with a cut-off set at a 1.5-fold change and a significance threshold of $P < 0.05$ [18,19]. Pathway enrichment analysis was carried out using cluster Profiler (R packages v4.6.0) to examine the KEGG pathways [20]. Enrichment analysis for Gene Ontology (GO) was conducted by utilizing GSEABase (R packages v1.60.0). Plots were generated using enrichplot (v1.18.3), ggplot2 (v3.4.1), cowplot (v1.1.1), and pheatmap (v1.0.12) packages. The RNA sequencing (RNA-seq) data reported in this paper have been deposited into sequence read archive (SRA) database under BioProject accession number PRJNA1053606 (https://trace.ncbi.nlm.nih.gov/Traces/study/?acc=PRJNA1053606&o=acc_s%3Aa).

2.11. RT-qPCR

After extracting total RNA from the hearts using RNAiso plus reagent (9108, TaKaRa, Dalian, China) according to the manufacturer's instructions [21], cDNA was obtained using the PrimeScriptTM RT reagent Kit with gDNA Eraser (RR047A, Takara, China). Subsequently, real-time quantitative reverse transcription polymerase chain reaction (RT-qPCR) was conducted using the SYBR Premix Ex Taq II (RR820A, TaKaRa, China) to detect the levels of targeted mRNAs with the 7900HT Fast RealTime PCR system (Applied Biosystems). GAPDH was utilized as the internal control. Each reaction was performed in triplicate. The values were normalized to GAPDH to calculate the relative RNA expression levels. The primer sequences used for mRNA expression detection are listed in Supplementary Table S1.

2.12. Transmission electron microscopy

The hearts were prefixed with 3% glutaraldehyde and then postfixed with 1% osmium tetroxide. They were dehydrated in a series of acetone solutions, infiltrated with Epon 812 for an extended period, and finally embedded. The semithin sections were stained with methylene blue, while ultrathin sections were cut using a diamond knife and stained with uranyl acetate and lead citrate. The sections were examined using a JEM-1400FLASH Transmission Electron Microscope.

2.13. Mitochondrial assays

The JC-1 mitochondrial membrane potential assay kit (C2003S, Beyotime) was utilized to measure the mitochondrial membrane potential (MMP). Following a single wash with PBS, the cells were incubated with 500 μL of staining working buffer per well for 20 min. After two washes with staining buffer solution, the covering liquid was replaced with Dulbecco's Modified Eagle Medium (DMEM) (11965092, Thermo Fisher Scientific). Finally, the cell fluorescence was observed using a fluorescence microscope. The mitochondrial permeability transition pore (PT-pore) assay kit (C2009S, Beyotime) was used to detect the opening of PT-pore. Each well was incubated with 500 μL of staining working solution for 30 min, followed by replacing the incubation liquid with pre-warmed DMEM and incubating further for 30 min under light-avoiding conditions. The nuclei were counterstained with Hoechst33342 (C1017, Beyotime). Subsequently, the cell fluorescence was observed under a fluorescence microscope after two washes with PBS.

Mitotracker Red (M7512, ThermoFisher Scientific) was preloaded into live cells before conducting immunofluorescence experiments. Subsequently, immunocytochemistry was carried out. Using Image J software, a blinded quantitative study of the fluorescence intensity was performed.

2.14. Cell culture

Neonatal (1-3 day-old) Sprague-Dawley rats were used to isolate primary ventricular cardiomyocytes (NRVMs) [22]. Briefly, neonatal rats were anesthetized by isoflurane and then euthanized by cervical dislocation. The hearts were removed and immediately placed in ADS buffer (pre-cooled, composed of 120 mmol/L NaCl, 20 mmol/L HEPES, 8 mmol/L NaH_2PO_4, 6 mmol/L glucose, 5 mmol/L KCl, 0.8 mmol/L $MgSO_4$, pH 7.4). Subsequently, the hearts were transferred into fresh ADS buffer and diced into pieces smaller than 1 mm^3. Then, the heart tissues were repetitively rinsed with sterile ADS until the rinse fluid became clear. The tissues were gathered and placed into a sterile 25 ml bottle along with 2 ml of collagenase II solution and 2 ml of ADS. The digestion process was conducted by continuously agitating the mixture at a speed of 180 rpm, maintained at a temperature of 37 °C, for an 8-min-duration. The suspensions were filtered into 50 ml centrifuge tubes that were kept chilled in ice. Into each tube, 1 ml of fetal bovine

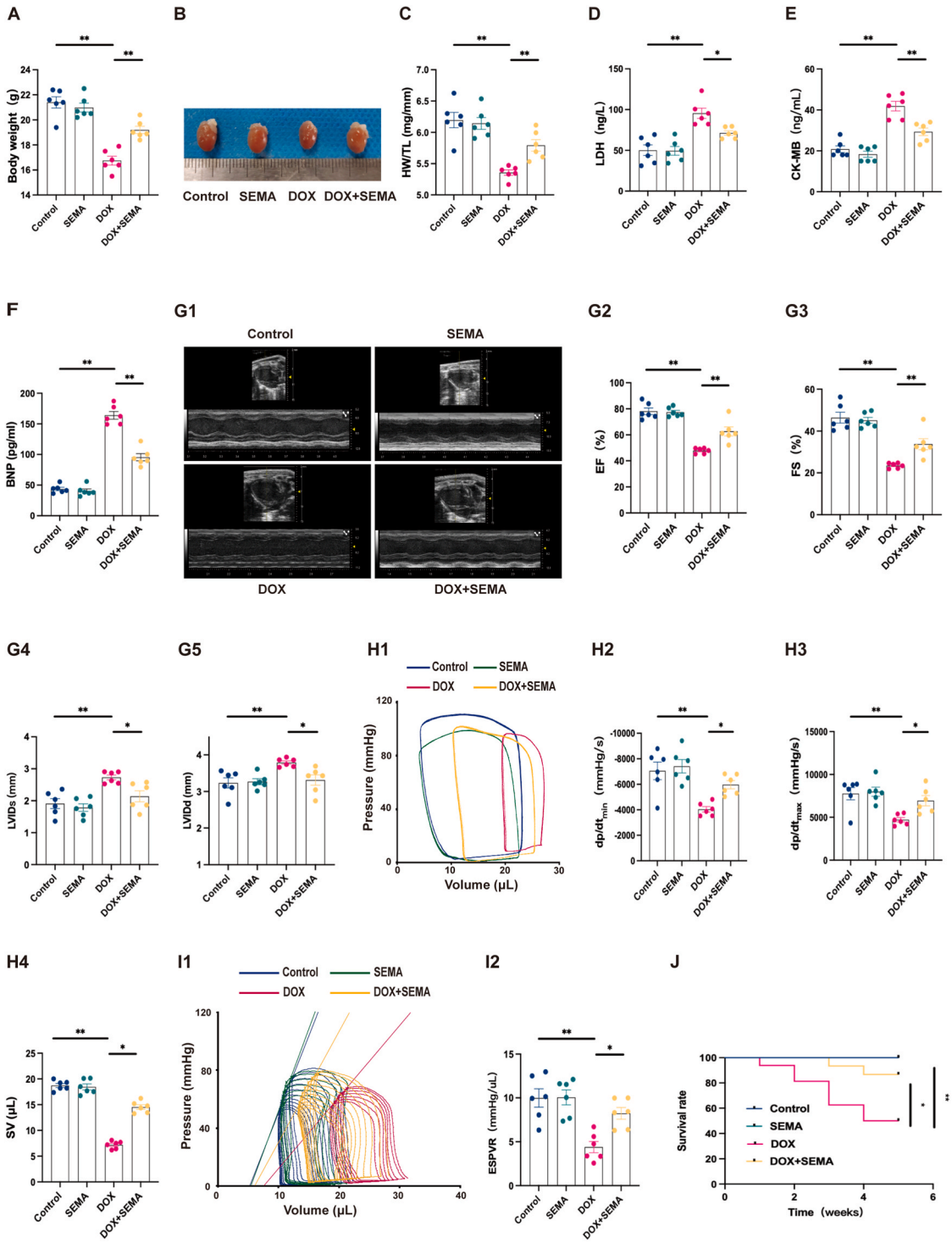

Fig. 1. SEMA ameliorates doxorubicin-induced cardiac dysfunction. C57/BL6J mice were used to establish a mouse model of doxorubicin-induced myocardial injury by the intraperitoneal (i.p.) injection of doxorubicin (5 mg/kg/week) for 4 weeks. Before the induction of cardiac dysfunction by doxorubicin treatment, semaglutide (SEMA,12 μg/kg/day) was subcutaneously injected daily for one week and continued for another 5 weeks, including one week after the last doxorubicin injection, after which time the parameters were collected. **A-C**: Body weight (A), representative whole heart pictures (B), and the ratio of heart weight to tibia length (HW/TL) (C) (n = 6 per group). **D-F:** Serum levels of lactate dehydrogenase (LDH), creatine kinase-MB (CK-MB), and brain natriuretic peptide (BNP) (n = 6 per group). **G**: Cardiac function determined by echocardiography, including typical M-mode echocardiogram pictures, left ventricular ejection fraction (EF%), left ventricular fractional shortening (FS%), left ventricular internal dimension-systole (LVIDs), and left ventricular internal dimension-diastole (LVIDd) (n = 6 per group). **H and I:** Cardiac function determined by invasive hemodynamics, including representative left ventricular pressure-volume (P-V) loops at steady state, dp/dt_{min} (maximal relaxation rate), dp/dt_{max} (maximum rate of pressure development), stroke volume (SV), representative left ventricular end-systolic pressure volume relationship (ESPVR) slope and load independent parameters of LV function: ESPVR (n = 6 per group). **J**: Mouse survival rates during the six week-experimental period (n = 15 per group). Statistical analysis was performed using one-way ANOVA, followed by Tukey's post-hoc test (A, C-I). Kaplan-Meier survival analysis was used to evaluate the survival rate of mice, and the results were compared using the log-rank test (J). *$p < 0.05$, **$p < 0.01$.

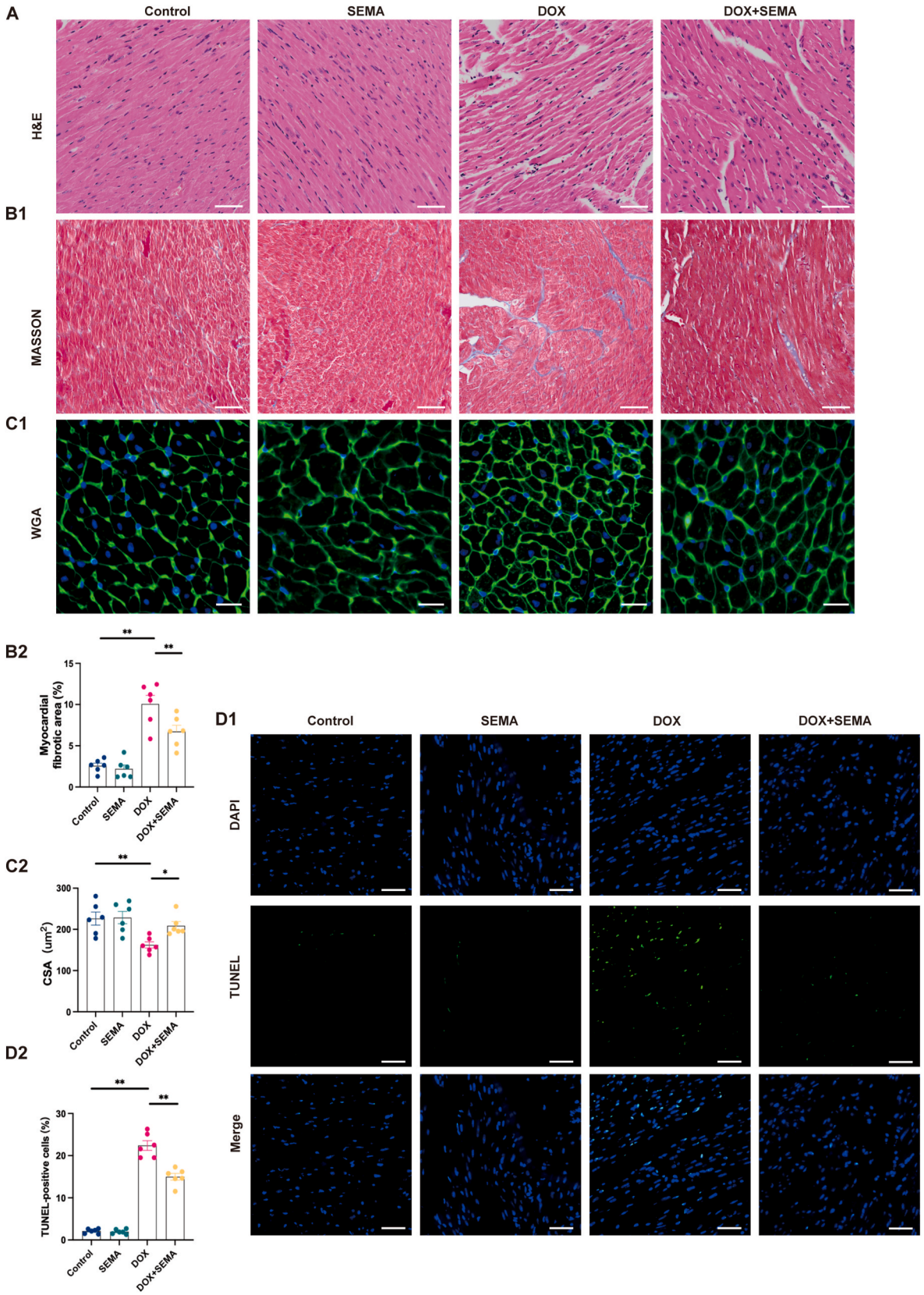

Fig. 2. SEMA attenuates doxorubicin-induced myocardial damage. Doxorubicin (DOX)-induced cardiac dysfunction was established as shown in Fig. 1, and then the hearts were harvested for histological analyses. **A:** H&E staining for the assessment of myocardial injury. Scale bar = 50 μm. **B:** Masson staining for the assessment of myocardial fibrosis. Scale bar = 50 μm. Representative image (B1) and quantification (B2) of the myocardial fibrotic area (n = 6 per group). **C:** Wheat germ agglutinin (WGA) staining for the assessment of myocyte size. Scale bar = 20 μm. Representative image (C1) and quantification (C2) of cross-sectional area (CSA) (n = 6 per group). **D**: TUNEL staining for the assessment of apoptosis. Scale bar = 20 μm. Representative images (D1) and quantification (D2) of TUNEL-positive cardiomyocytes (n = 6 per group). Statistical analysis was performed using one-way ANOVA, followed by Tukey's post-hoc test. *p < 0.05, **p < 0.01.

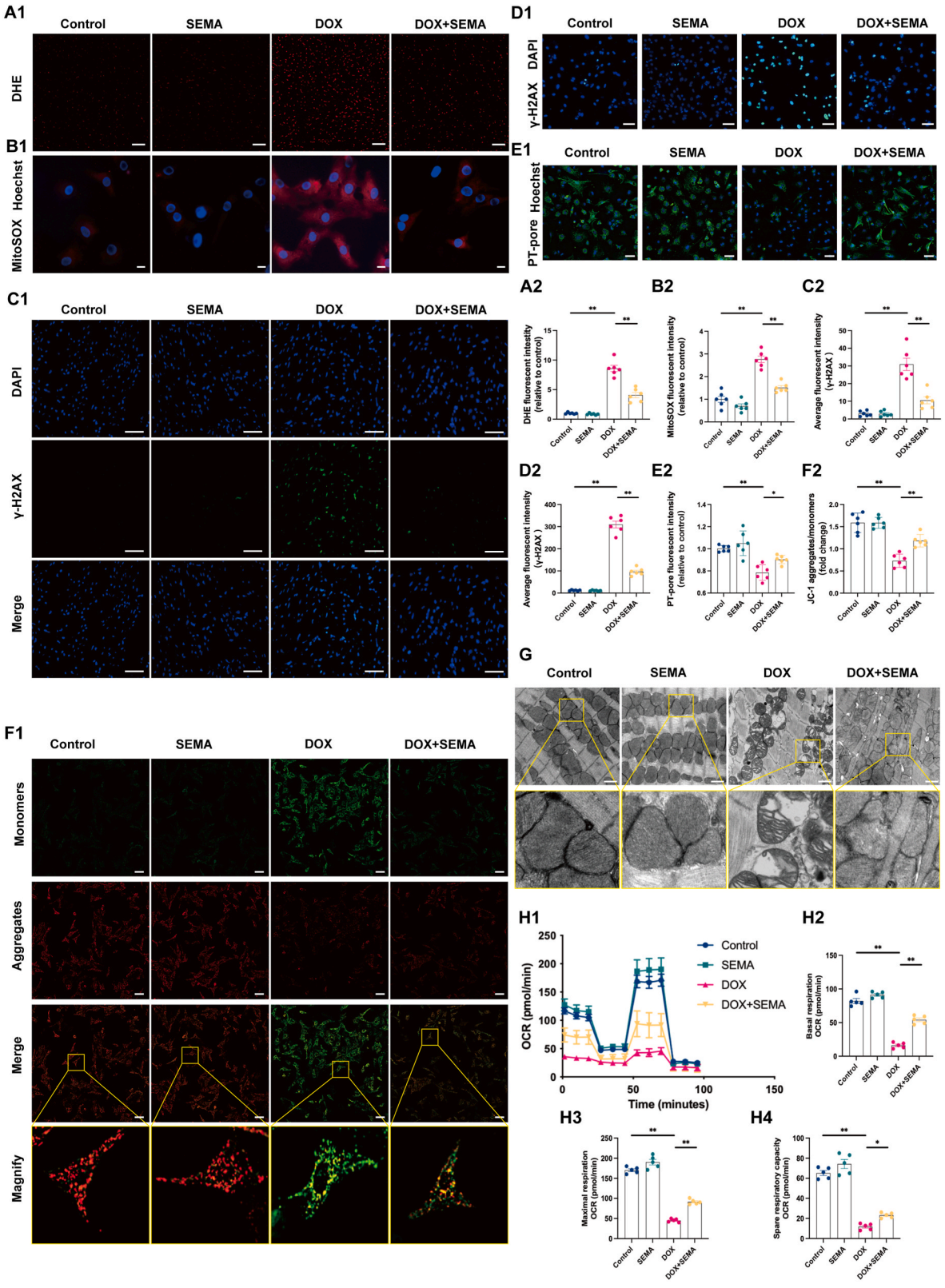

(caption on next page)

Fig. 3. SEMA suppresses cardiomyocyte oxidative stress and attenuates mitochondrial damage. Doxorubicin (1 μM) or saline (vehicle) was used to treat primary cardiomyocytes for 24 h with/without combined incubation of semaglutide (SEMA, 1 nM). The cardiomyocytes were pre-incubated in the incubation medium for 2 h before exposure to doxorubicin. **A and B:** Total reactive oxygen species (ROS) levels *in vivo,* measured by DHE (**A**) and mitochondrial ROS levels *in vitro* measured by MitoSOX Red **(B).** Representative images (A1 and B1) and quantifications (A2 and B2) of ROS levels (n = 6 per group). DHE staining: scale bar = 50 μm. MitoSOX staining: scale bar = 10 μm. **C and D**: Immunofluorescence images of γ-H2AX *in vivo* **(C)** and *in vitro* **(D)**. Representative images (C1 and D1) and quantifications (C2 and D2) of fluorescence intensity for γ-H2AX (n = 6 per group), Scale bar = 50 μm. **E**: Fluorescent images of mitochondrial permeability transition pore (PT-pore) (fluorescence intensity is negatively correlated with PT-pore opening). Representative image (E1) and quantification (E2) of PT-pore fluorescence intensity (n = 6 per group), Scale bar = 50 μm. **F**: JC-1 staining for assessment of mitochondrial membrane potential (MMP). Representative image (F1) and quantification (F2) of JC-1 aggregates/monomers (n = 6 per group), Scale bar = 50 μm. **G**: Representative transmission electron microscopy images of mitochondrial morphology of cardiac muscle. Scale bar = 1 μm. H: Mitochondrial oxygen consumption rate (OCR) of primary cardiomyocytes. Representative image (H1) and quantification (H2 - H4) of basal respiration, maximal respiration, and spare respiratory capacity (n = 5 per group). Statistical analysis was performed using one-way ANOVA, followed by Tukey's post-hoc test. *p < 0.05, **p < 0.01. (For interpretation of the references to colour in this figure legend, the reader is referred to the Web version of this article.)

serum (FBS, Gibco) was added. After a 5-min centrifugation at 2000 g, the supernatant was discarded. The pellets were suspended in FBS and subsequently seeded into a petri-dish. The dish was incubated at 37 °C, with a CO_2 concentration of 5%, for a period of 2 h. This process allowed for the separation of cardiomyocytes and fibroblasts. Then, the supernatant was carefully transferred into a 50 ml centrifuge tube. High purity cardiomyocytes were isolated from fibroblasts by employing a Percoll gradient (GE17-0891-01, Sigma-Aldrich) in sterile ADS buffer. Following centrifugation at 1800 g for 45 min, the cardiomyocytes were separated and placed in the intermediate layer. The isolated cells were then cultured in a 5% CO_2 incubator at 37 °C for 24 h using DMEM supplemented with 10% FBS and 1% penicillin-streptomycin.

The primary cardiomyocytes were incubated in a microplate, and then infected with the AAV9 (Hanbio Biotechnology, Shanghai, China). The medium was replaced 6–8 h after infection, and subsequent treatments were performed after 24 h.

2.15. Mitochondrial fractionation, western blot analyses, and immunoprecipitation

Mitochondrial and cytoplasmic fractions were extracted from cardiomyocytes using the Cell Mitochondria Isolation kit (C3601, Beyotime Biotechnology). Protein expression levels in both cardiac tissues and NRVMs were measured by Western blot analysis. Total protein samples were collected, and their concentrations were measured using a BCA protein assay kit (PC0020, Solarbio). Afterwards, 50 mg of the protein samples were subjected to SDS-PAGE for separation and then transferred onto nitro-cellulose membranes (GE Healthcare Life Sciences, Logan, UT). To block non-specific binding, the membranes were treated with 5% non-fat milk for 1 h and then incubated overnight at 4 °C with the corresponding primary antibodies. The blotted membranes were probed with the following antibodies, that included rabbit anti-BNIP3 antibody (1: 1,000, ab109362, Abcam), rabbit anti-PI3K p85 antibody (1: 1,000, ab191606, Abcam), rabbit anti-p-PI3K p85 antibody (1: 1,000, ab182651, Abcam), rabbit anti-AKT antibody (1:1,000, 4691T, Cell Signaling Technology, Danvers, MA), rabbit anti-p-AKT antibody (1:1,000, 4060T, Cell Signaling Technology), rabbit anti-VDAC1 antibody (1:5000, ab154856, Abcam), and rabbit anti-GAPDH antibody (1:10,000, 10494-1-AP, Proteintech, Wuhan, China). Following incubation, the membranes were washed with a wash buffer to remove any excess primary antibodies. Fluorescent-labeled goat anti-rabbit IgG (5151, Cell Signalling Technology) was then used to detect the primary antibodies, and the resulting protein bands were visualized using the Odyssey Western Blot Detection System (LI-COR Biotechnology, Lincoln, Nebraska, NE). The relative protein expression levels were determined based on the gray intensity of the bands. Phosphorylated BNIP3 was detected by immunoprecipitation. The cell lysates were immunoprecipitated with phospho-Ser/Thr antibody (Abcam, ab17464) and then immunoblotted with anti-BNIP3 antibody. For immunoprecipitation, IgG was used as negative control (NC) and anti-BNIP3 antibody was used as positive control (PC)

2.16. Statistical analysis

The data are presented as mean ± SEM. GraphPad Prism 9.0 (GraphPad Software) was used for statistical analyses. Experiments were independently conducted at least 3 times, with specific N numbers and technical replicates provided in each figure. Variance between groups was assessed using a Brown-Forsythe test, which showed no significant differences. One-way analysis of variance (ANOVA) was used to compare more than two groups, followed by Tukey's post-hoc test when different groups were compared among each other. Differences between the two groups were assessed using a 2-tailed unpaired Student's t-test. Survival analysis was performed utilizing the Kaplan-Meier method, and the outcomes were subsequently compared using the log-rank test.

3. Results

3.1. Semaglutide ameliorates doxorubicin-induced cardiac dysfunction

To investigate the potential role of semaglutide in doxorubicin-induced cardiotoxicity, we established a mouse model of chronic doxorubicin-induced myocardial injury (Fig. S1A). Consistent with other reports [23], the doxorubicin (i.p. 5 mg/kg/week) mouse model has decreased body weight, heart size, and heart weight/tibia length ratio (Fig. 1A-C), and increased serum levels of lactate dehydrogenase (LDH) and creatine kinase MB (CK-MB) (Fig. 1D-E). The cardiac function was impaired by doxorubicin, shown by increased serum brain natriuretic peptide (BNP) concentration (Fig. 1F), and decreased left ventricular ejection fraction (LVEF) and left ventricular fractional shortening (LVFS) and increased left ventricular internal dimension-systole (LVIDs) and left ventricular internal dimension-diastole (LVIDd) (Fig. 1G). Furthermore, doxorubicin induced a rightward shift in the steady-state pressure-volume (P-V) loop and led to a reduction in dp/dt_{min}, dp/dt_{max}, and stroke volume (SV) (Fig. 1H). In addition, there was a decrease in the slope of the LV end-systolic pressure-volume relationship (ESPVR) (Fig. 1I) acquired during variable loading, subsequent to inferior vena cava occlusion in doxorubicin-treated mice. The doxorubicin-mediated impairment in cardiac function may have contributed to the decreased survival rate relative to the control group (Fig. 1J). The above-mentioned aberrant parameters were almost completely abrogated by semaglutide (s.c. 12 μg/kg/day) (Fig.1A-J).

The functional data were corroborated by histopathological studies. Doxorubicin caused severe myocardial fiber breakdown and disorder, shown by H&E staining (Fig. 2A), accompanied with increased interstitial fibrosis and decreased cardiomyocyte cross-sectional area, shown by Masson trichrome and WGA staining (Fig. 2B-C). These histopathological aberrations caused by doxorubicin were partially or completely reversed by semaglutide treatment. TUNEL staining also showed that semaglutide decreased the increased apoptosis of cardiomyocytes in doxorubicin-treated mice (Fig. 2D), which may, at least in part, account for the protective effects of semaglutide on doxorubicin-induced cardiotoxicity.

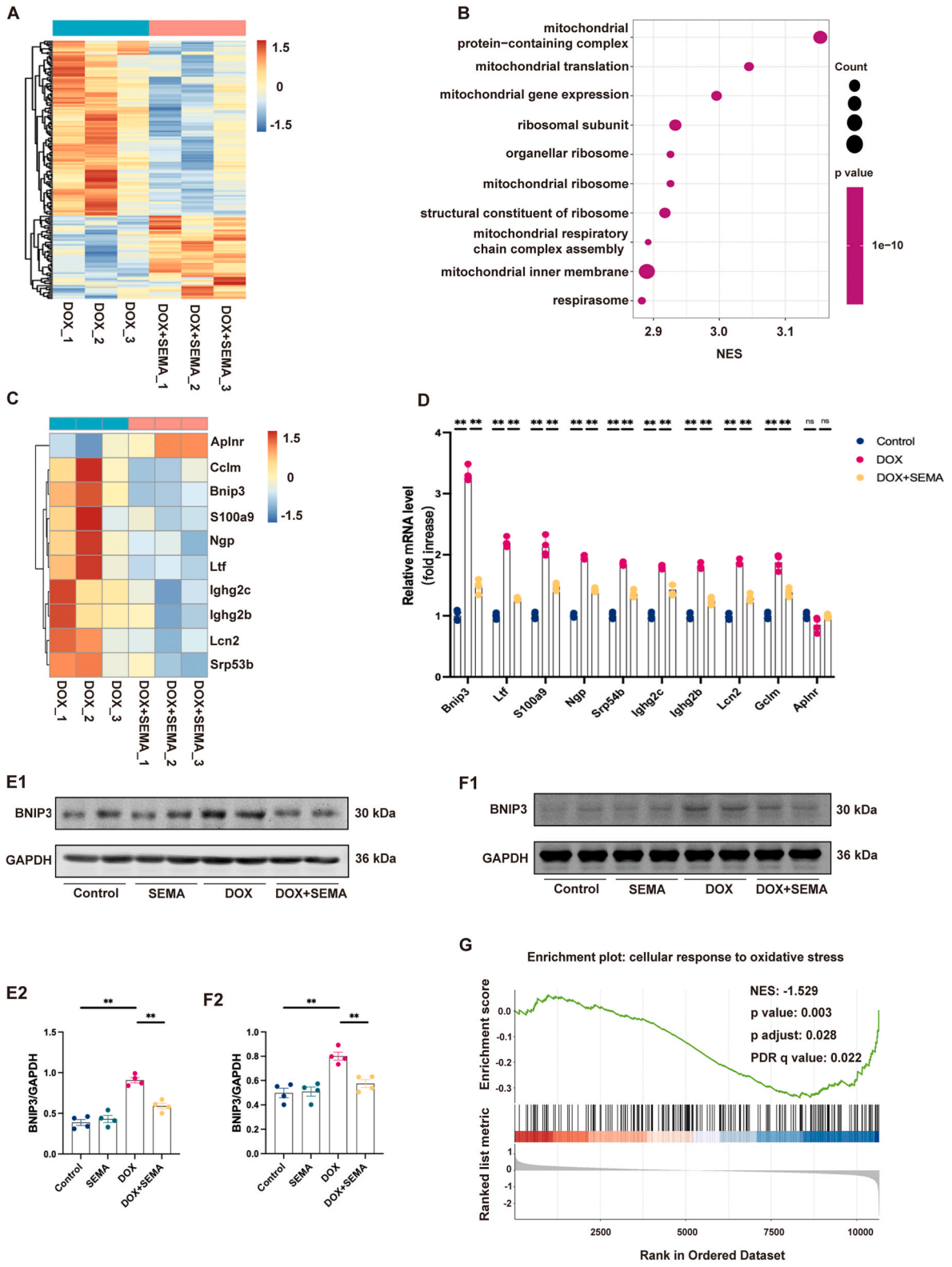

Fig. 4. SEMA via Bnip3, ameliorates doxorubicin-induced myocardial mitochondrial dysfunction. Doxorubicin (DOX)-induced cardiac dysfunction was established as that in Fig. 1, and then the hearts were harvested for further analyses. **A**: Heatmap of the differentially expressed genes in the myocardium (n = 3 per group) (Fold change ≥ ± 1.5, p value < 0.05). **B**: Bubble plot of the top 10 categories enriched in GO analysis via GSEA, arranged in the descending order of the absolute value of the normalized enrichment score (NES) (|NES|> 1, q value < 0.25). **C:** Heatmap of the top 10 differentially expressed genes based on log-fold change. **D:** qPCR validation of the top 10 genes in Figure C (n = 4 per group). **E and F:** Western blots of BNIP3 expression in lysates from C57/BL6J mouse hearts and NRVMs. Representative blot (E1 and F1) and quantitative data are shown (E2 and F2) (n = 4 per group). **G:** Gene enrichment plot illustrating the cellular response to oxidative stress pathway involving BNIP3 analyzed by GSEA (|NES|> 1, q value < 0.25). Statistical analysis was performed using one-way ANOVA, followed by Tukey's post-hoc test. *p < 0.05, **p < 0.01.

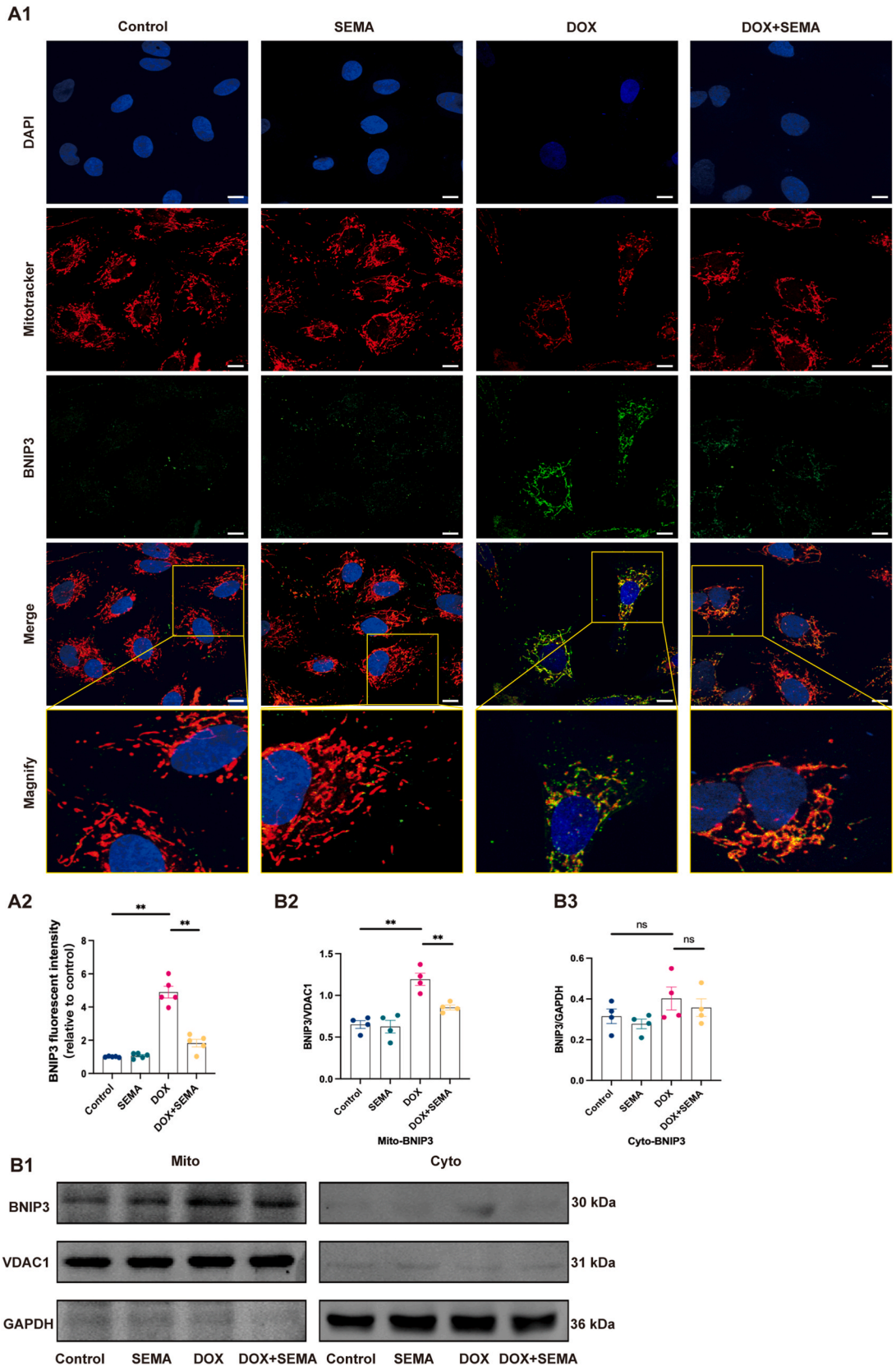

Fig. 5. SEMA suppresses BNIP3 expression in the mitochondria. Primary cardiomyocytes were treated as that in Fig. 3. **A:** Immunofluorescence of the colocalization of BNIP3 (green) with Mitotracker Red (mitochondria). Representative image (A1) and quantification (A2) of fluorescence intensity for BNIP3 (n = 5 per group). Scale bar = 10 μm. **B:** Representative western blots in the determination of the cytoplasmic and mitochondrial levels of BNIP3 (B1) and quantitative data of mito-BNIP3/VDAC1 and cyto-BNIP3/GAPDH protein levels (B2 and B3) (n = 4 per group). cyto = cytoplasm; mito = mitochondria. Statistical analysis was performed using one-way ANOVA, followed by Tukey's post-hoc test. *p < 0.05, **p < 0.01. (For interpretation of the references to colour in this figure legend, the reader is referred to the Web version of this article.)

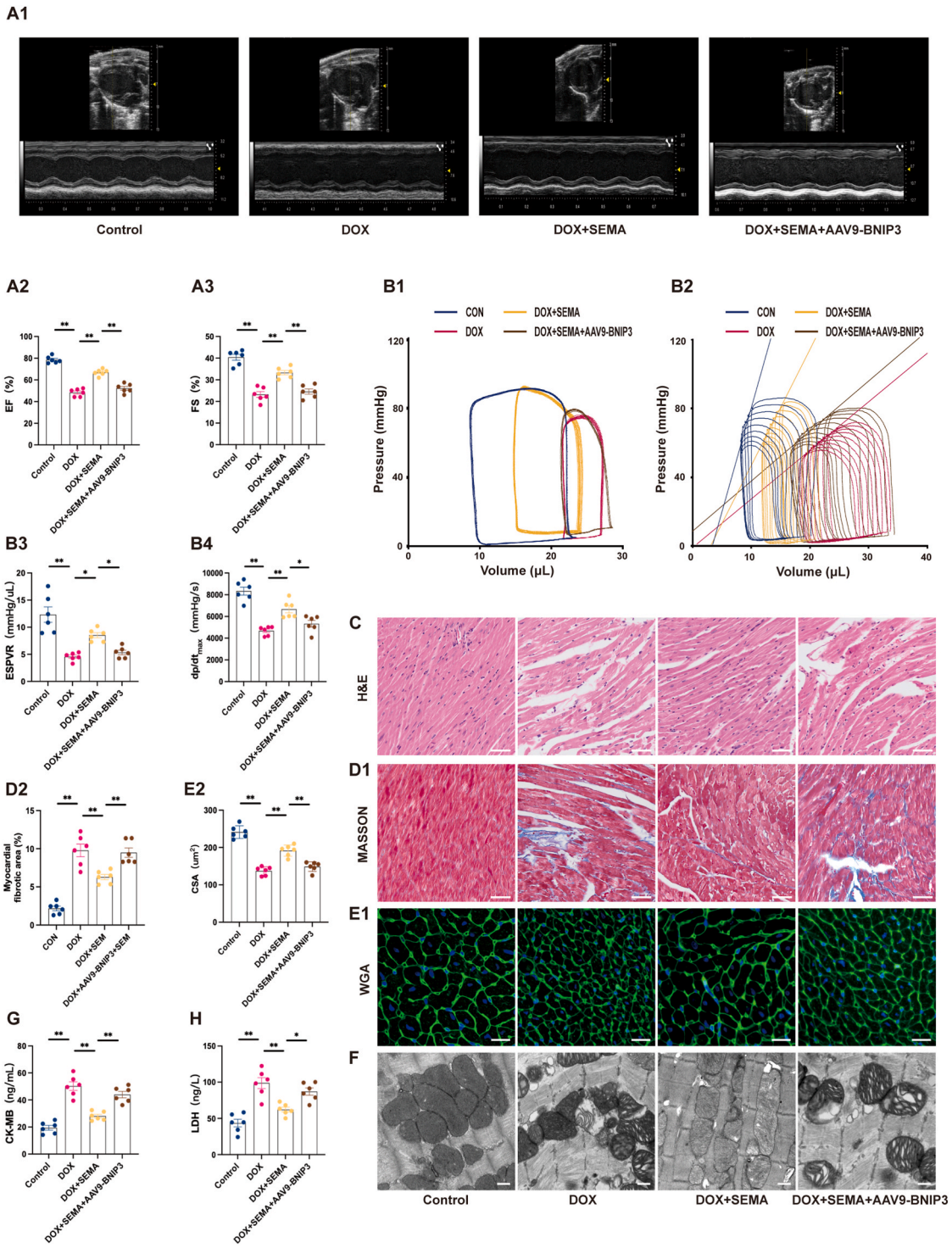

Fig. 6. BNIP3 blocks the amelioration of cardiac function induced by SEMA. C57/BL6J mice, infected with AAV9-BNIP3 or AAV9-EGFR for four weeks, were subjected to 4 weeks of the intraperitoneal injection of saline (vehicle) or doxorubicin (DOX) with/without combined administration of semaglutide (SEMA) for 6 weeks (as in Supplemental Fig. S1B), and then the parameters were collected. **A:** Cardiac function determined by echocardiography, including typical M-mode echocardiogram pictures, LVEF (%), LVFS (%) (n = 6 per group). **B:** Cardiac function determined by invasive hemodynamics, including representative left ventricular pressure-volume (P-V) loops at steady state, representative left ventricular end-systolic pressure volume relationship (ESPVR) slope, load independent parameters of LV function: ESPVR, and dp/dt_{max} (maximum rate of pressure development) (n = 6 per group). **C:** H&E staining for assessment of myocardial injury. Scale bar = 50 μm. **D:** Masson staining for assessment of myocardial fibrosis. Scale bar = 50 μm. Representative image (D1) and quantification (D2) of the myocardial fibrotic area (n = 6 per group). **E:** Wheat germ agglutinin (WGA) staining for assessment of cardiomyocyte size. Scale bar = 20 μm. Representative image (E1) and quantification (E2) of cross-sectional area (CSA) (n = 6 per group). **F:** Representative transmission electron microscopy images of mitochondrial morphology of cardiac muscle. Scale bar = 500 nm. **G and H**: Serum levels of creatine kinase-MB (CK-MB) and lactate dehydrogenase (LDH) (n = 6 per group). Statistical analysis was performed using one-way ANOVA, followed by Tukey's post-hoc test. *$p < 0.05$, **$p < 0.01$.

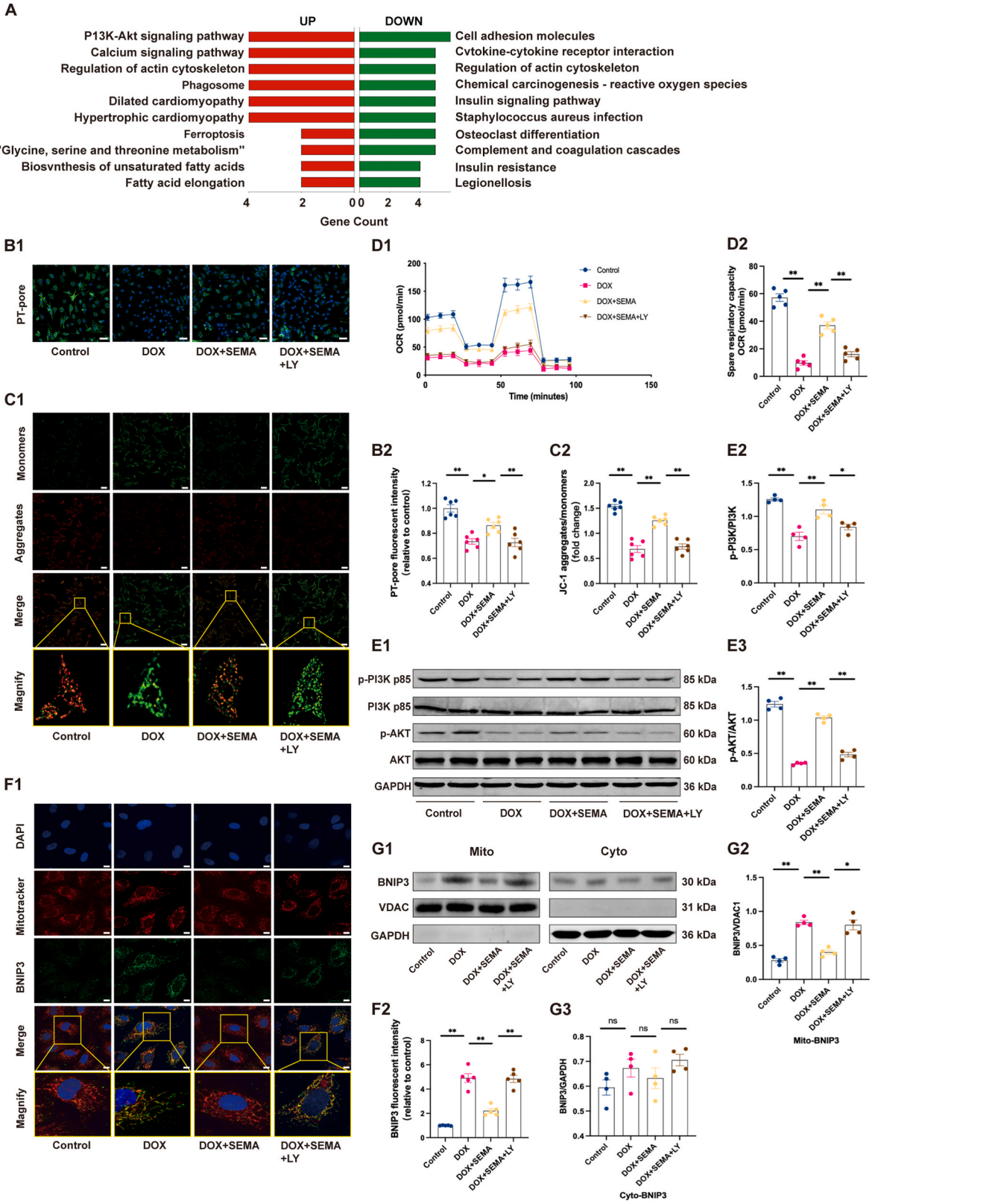

(caption on next page)

Fig. 7. SEMA attenuates doxorubicin-induced mitochondrial injury through regulation of the PI3K/AKT/BNIP3 pathway. Primary cardiomyocytes were pretreated with saline (vehicle) or semaglutide (SEMA, 1 nM) for 2 h before cotreatment with/without doxorubicin (DOX, 1 μM) for 24 h with or without LY294002 (LY, 10 μM) also for 24 h. **A:** The top 10 up-regulated and down-regulated pathways analyzed by KEGG enrichment using the RNA-sequencing data. **B:** Fluorescent images of mitochondrial permeability transition pore (PT-pore) (fluorescence intensity is negatively correlated with PT-pore opening). Scale bar = 50 μm. Representative image (B1) and quantification (B2) of PT-pore fluorescence intensity (n = 6 per group). **C:** JC-1 staining for the assessment of MMP. Scale bar = 50 μm. Representative image (C1) and quantification (C2) of JC-1 aggregates/monomers (n = 6 per group). **D:** Mitochondrial oxygen consumption rate (OCR) of primary cardiomyocytes. Representative image (D1) and quantification (D2) of spare respiratory capacity (n = 5 per group). **E:** Representative western blots (E1) and quantitative data on the protein levels of p-PI3K/PI3K, p-AKT/AKT (E2 and E3) (n = 4 per group). **F:** Immunofluorescence of the colocalization of BNIP3 (green) with Mitotracker Red (mitochondria). Scale bar = 10 μm. Representative image (F1) and quantification (F2) of fluorescence intensity of BNIP3 (n = 5 per group). **G:** Representative western blots (G1) to determine the cytoplasmic and mitochondrial levels of BNIP3 protein and quantitative data for mito-BNIP3/VDAC1 and cyto-BNIP3/GAPDH protein levels (G2 and G3) (n = 4 per group). cyto = cytoplasm; mito = mitochondria. Statistical analysis was performed using one-way ANOVA, followed Tukey's post-hoc test. *$p < 0.05$, **$p < 0.01$. (For interpretation of the references to colour in this figure legend, the reader is referred to the Web version of this article.)

3.2. Semaglutide protects cardiomyocytes against doxorubicin-induced injury by improvement of mitochondrial function

The results of the *in vivo* experiments were corroborated by the *in vitro* experiments. In cardiomyocytes in primary culture semaglutide reduced the doxorubicin-mediated decrease in cell viability, determined by calcein in a concentration-dependent manner (Figs. S2A and S2B). Based on the concentration response studies, 1 nM was chosen as the working concentration for semaglutide in subsequent experiments. Doxorubicin decreased cell viability of cardiomyocytes (Figs. S2A and S2B), and increased LDH concentration in the culture medium, which were reversed by semaglutide (Figs. S2A–S2C). Due to the role of reactive oxygen species (ROS) and DNA damage in the doxorubicin-induced cardiotoxicity [24,25], we measured the levels of ROS and γ-H2AX, a DNA double-strand break marker, in the cardiomyocytes. We found that doxorubicin increased ROS levels and γ-H2AX expressions *in vivo* (Fig. 3A and C) and *in vitro* (Fig. 3B and D), which were reversed by semaglutide (Fig. 3A-D). It is known that doxorubicin-induced increase in ROS is via a detrimental effect on the mitochondria [26]. To investigate whether mitochondrial ROS contributes to doxorubicin-induced cardiac damage, we used mitoTEMPO, a mitochondrially targeted antioxidant, in doxorubicin-treated cardiomyocytes. Our results showed that mitoTempo reduced the doxorubicin-induced cell mortality and LDH release (Figs. S2D–S2E), confirming the significance of mitochondrial ROS in doxorubicin-induced cardiomyocyte dysfunction. Our present study also showed that doxorubicin increased the permeability transition (PT)-pore opening (Fig. 3E), decreased mitochondrial membrane potential (MMP), assessed by JC-1 aggregate levels (Fig. 3F) and caused morphological defects of the mitochondria in the cardiomyocytes, as evidenced by distorted and reduced cristae density (Fig. 3G). Furthermore, we used extracellular flux analysis to monitor in real-time mitochondrial respiratory capacity *in vitro*. Doxorubicin markedly reduced mitochondrial oxygen consumption rate (OCR), basal and maximal respiration, and spare respiratory capacity, as well (Fig. 3H). In the presence of semaglutide, the above-mentioned changes were ameliorated (Fig. 3E-H), suggesting that semaglutide ameliorates doxorubicin-induced cardiac injury via improvement of mitochondrial function.

3.3. Semaglutide, via Bnip3, ameliorates doxorubicin-induced mitochondrial and cardiac dysfunction

To explore further the mechanisms underlying the protective effect of semaglutide on doxorubicin-induced cardiotoxicity, RNA-seq was carried out to explore the potential transcriptional alterations induced by semaglutide (Fig. 4A). We used GO-related gene set enrichment analysis (GSEA) to search for the function-expression associations. We found that the top 10 GO terms were mainly related to mitochondrial-related functions (Fig. 4B). Differentially expressed genes (DEGs) with the cut-off set at a 1.5-fold change and a significance threshold of P-value <0.05 were searched. The top 10 DEGs with the greatest absolute rank-normalized log-fold change (logFC) values between groups are listed in the heatmap (Fig. 4C). Then, we performed qRT-PCR of mouse myocardial tissue to validate the expression of the top 10 DEGs and found that the gene with the highest expression was Bnip3 (Fig. 4D), which was confirmed by immunoblotting the hearts in the *in vivo* and NRVMs in the *in vitro* studies (Fig. 4E and F). Furthermore, GSEA confirmed the cellular response via the oxidative stress pathway, where the *Bnip3* gene is located, was inhibited, further indicating the potential functional role of BNIP3 in the semaglutide-mediated amelioration of doxorubicin-induced mitochondrial dysfunction (Fig. 4G).

Recent studies revealed that hypoxia induces the integration of the death protein BNIP3 in the mitochondria by its carboxyl-terminal transmembrane domain to trigger mitochondrial injury on the inner mitochondrial membrane, resulting in PT-pore opening, loss of MMP, and cell death of cardiac myocytes [27,28]. Our results showed that doxorubicin caused an increase in BNIP3 expression in the mitochondria, which was mitigated by semaglutide (Fig. 5A and B). To further show the role of BNIP3 on the semaglutide-mediated protection, AAV9-BNIP3 or AAV9-EGFP (enhanced green fluorescent protein) driven by the cardiac troponin T promoter was injected into the tail veins of C57/BL6J mice at a concentration of 5×10^{10} viral genome per mouse to over-express BNIP3 (Fig. S1B). Four weeks after the injection of AAV9, the successful infection was detected by EGFP fluorescence and increased BNIP3 expression in cardiomyocytes from the AAV9-BNIP3 group (Figs. S3A and S3B). Moreover, at the end of experiment, we also detected the BNIP3 overexpression in each group by western blot (Fig. S3C). BNIP3 overexpression impaired the semaglutide-mediated cardiac protection in doxorubicin-induced heart dysfunction (Fig. 6A and B). The beneficial effects of semaglutide on myocardial fiber disorder, interstitial fibrosis, and myocardial cell cross-sectional area in the myocardium were blocked by overexpression of BNIP3 (Fig. 6C-E). Transmission electron microscopy also showed that overexpression of BNIP3 reduced the protective effect of semaglutide on mitochondrial morphology (Fig. 6F). BNIP3 overexpression recouped the lowered serum levels of LDH and CK-MB induced by semaglutide (Fig. 6G and H). Moreover, the semaglutide-mediated amelioration of the doxorubicin-induced reduction in mitochondrial respiratory capacity was blocked by BNIP3 overexpression. (Fig. S4A).

3.4. semaglutide attenuates the doxorubicin-induced mitochondrial injury through the PI3K/AKT/BNIP3 pathway

By further analyzing the aforementioned RNA-seq data (Fig. 4A), we observed a significant upregulation of the PI3K/Akt pathway in the semaglutide-treated doxorubicin group compared with the doxorubicin

group (Fig. 7A). To show the role of PI3K/AKT pathway on semaglutide-mediated modulation of BNIP3 expression, we used LY294002 as a PI3K inhibitor in the present study [29]. We found that LY294002 blocked the ability of semaglutide to mitigate the doxorubicin-induced mitochondrial ROS generation (Fig. S5A), PT-pore opening (Fig. 7B, Fig. S5B), as well as the reduction of MMP and OCR. (Fig. 7C and D). Western blots showed that semaglutide reversed the doxorubicin-induced down-regulation of p-PI3K and p-AKT. However, in the presence of LY294002, the semaglutide-mediated upregulation of p-PI3K disappeared (Fig. 7E). Moreover, LY294002 did not affect BNIP3 phosphorylation (Fig. S5C). Additionally, confocal microscopy and western blot showed that the doxorubicin-mediated increase in BNIP3 that was decreased by semaglutide was restored by LY294002 (Fig. 7F and G). These findings suggested that semaglutide reduces the damage caused by doxorubicin to the mitochondria by stimulating PI3K/AKT to decrease the expression of BNIP3 in the mitochondria.

4. Discussion

Doxorubicin, a commonly clinically used drug for treating malignant tumors, has shown significant efficacy. However, its side effects could not be ignored. One of the major concerns is its cardiotoxicity, and the prolonged use of doxorubicin can increase the risk of heart failure [30]. Potential cardioprotective agents, such as antioxidants and anti-apoptotic substances, are only currently used in experimental settings and still far from use in clinical practice [31]. Our findings suggested that semaglutide could mitigate the cardiac dysfunction and myocardial injury induced by doxorubicin. This protective effect may be achieved through the PI3K/AKT/BNIP3 pathway.

GLP-1, an incretin secreted by L-cells in the intestine, has a promising potential for the treatment of diabetes [32,33]. Semaglutide is a long-acting GLP-1 analog, approved by the US Food and Drug Administration for treating type 2 diabetes [34]. Previous studies have demonstrated that semaglutide has both hypoglycemic and cardiovascular protective effects, which includes a decrease in myocardial infarct area, myocardial ischemia-reperfusion damage, and cardiac vasculitis, as well as the suppression of myocardial cell apoptosis [35–38]. Our present study showed that a promising cardio-protective effect of semaglutide may be the treatment of doxorubicin-induced cardiotoxicity.

Although the mechanisms underlying doxorubicin-induced cardiotoxicity are not fully understood, some proposed pathways include mitochondrial dysfunction, oxidative stress, disrupted autophagy, inflammation, ferroptosis, pyroptosis, and apoptosis [39–43]. Our present study found that doxorubicin impaired mitochondrial morphology and function, which was reversed by semaglutide. RNA-Seq showed that Bnip3 is the potential candidate gene mediating the protective effect of semaglutide in doxorubicin-induced cardiotoxicity mouse model. Bnip3 has been identified as a crucial regulator of mitochondrial function and cell death in cardiomyocytes following hypoxia, ischemia, and reperfusion [44,45]. A recent study has provided additional evidence supporting the role of Bnip3 as a molecular effector in doxorubicin-induced mitochondrial perturbations and necrotic cell death in cardiac myocytes [46]. Interestingly, bioinformatics, western blotting, and immunofluorescence in our study proved that semaglutide significantly inhibited the expression of BNIP3 which was increased by doxorubicin. Moreover, the overexpression of BNIP3 blocked the improvement in cardiac function caused by semaglutide, indicating that BNIP3 is the key signal in the protective effect of semaglutide on doxorubicin-induced cardiac injury.

A previous study found that GLP-1 improved myocardial ischemia by shrinking the infarct size via the PI3K-AKT signaling pathway [47]. GLP-1 has also been shown to enhance the endothelial proliferation and function in people with type 2 diabetes and coronary heart disease [48]. Besides, GLP-1 can also inhibit pancreatic beta cell death by activating the PI3K-AKT and PKA-ERK signaling pathways [49]. Our present study showed the engagement of the PI3K-AKT signaling pathway in the semaglutide-mediated protection of cardiac function. Immunoblotting showed that semaglutide activated the PI3K/AKT pathway; in the presence of LY294002, a PI3K inhibitor, the negative regulation of BNIP3 by semaglutide was blocked. Taken together, our present study indicates that semaglutide reduces doxorubicin-mediated cardiomyocyte mitochondrial injury by regulating the PI3K/AKT/BNIP3 pathway.

In conclusion, semaglutide reduces doxorubicin-induced mitochondrial and cardiac dysfunction via PI3K/AKT pathway. This pathway reduces BNIP3 expression in the mitochondria, improves mitochondrial function, and reduces doxorubicin-mediated cardiac injury and improves cardiac function. Therefore, semaglutide is a potential therapy to reduce doxorubicin-induced acute cardiotoxicity.

Authors' contributions

Chunyu Zeng, Li Guo and Xiaoping Li conceived the project. Jiangjiao Wu and Shengnan Chen performed bioinformatic analysis. Wenbin Luo, Junkai Zhang, Fengxian Wang and Yang Tang performed the experiments *in vitro*. Lu Zhou, Xiaoping Li and Yu Tao performed the experiments *in vivo*. Xiaoping Li, Yu Tao and Yang Tang analyzed the data. Pedro A Jose and Yu Huang provided technical expertise. Chunyu Zeng and Li Guo supervised the project. Chunyu Zeng, Li Guo and Xiaoping Li summarized the data and wrote the manuscript with feedback from all authors. The order of co–first authors was determined by the volume of work each contributed to the study.

Funding

These studies were supported in part by grants from the National Key R&D Program of China (2022YFA1104500); Program of Innovative Research Team by the National Natural Science Foundation (81721001); National Natural Science Foundation of China (81930008); National Institutes of Health (5R01DK119652 and 1R01DK134574).

CRediT authorship contribution statement

Xiaoping Li: Writing – review & editing, Writing – original draft, Formal analysis, Data curation, Conceptualization. **Wenbin Luo:** Methodology, Data curation. **Yang Tang:** Data curation. **Jiangjiao Wu:** Formal analysis. **Junkai Zhang:** Methodology, Data curation. **Shengnan Chen:** Data curation. **Lu Zhou:** Data curation. **Yu Tao:** Data curation. **Yuanjuan Tang:** Data curation. **Fengxian Wang:** Data curation. **Yu Huang:** Writing – review & editing, Supervision, Methodology. **Pedro A. Jose:** Writing – review & editing, Supervision. **Li Guo:** Supervision, Conceptualization. **Chunyu Zeng:** Writing – review & editing, Funding acquisition, Conceptualization.

Declaration of competing interest

The authors declare that they have no competing interests. This manuscript is an original contribution not previously published and not under consideration for publication elsewhere.

Data availability

Data will be made available on request.

Acknowledgments

We would like to thanks Wei Wang (Department of Cardiology, Daping Hospital) for useful discussion.

Appendix A. Supplementary data

Supplementary data to this article can be found online at https://doi.org/10.1016/j.redox.2024.103129.

References

[1] A.A. Dhir, S.P. Sawant, Cardiac morbidity & mortality in patients with breast cancer: a review, Indian J. Med. Res. 154 (2021) 199–209.

[2] E. Chuang, N. Wiener, P. Christos, R. Kessler, M. Cobham, D. Donovan, G. L. Goldberg, T. Caputo, A. Doyle, L. Vahdat, J.A. Sparano, Phase I trial of ixabepilone plus pegylated liposomal doxorubicin in patients with adenocarcinoma of breast or ovary, Ann. Oncol. 21 (2010) 2075–2080.

[3] L. Yu, W.K.K. Wu, Z.J. Li, Q.C. Liu, H.T. Li, Y.C. Wu, C.H. Cho, Enhancement of doxorubicin cytotoxicity on human esophageal squamous cell carcinoma cells by indomethacin and 4-[5-(4-chlorophenyl)-3-(trifluoromethyl)-1H-pyrazol-1-yl]benzenesulfonamide (SC236) via inhibiting P-glycoprotein activity, Mol. Pharmacol. 75 (2009) 1364–1373.

[4] R. Mattioli, A. Ilari, B. Colotti, L. Mosca, F. Fazi, G. Colotti, Doxorubicin and other anthracyclines in cancers: activity, chemoresistance and its overcoming, Mol. Aspect. Med. 93 (2023) 101205.

[5] M.D.A. Paskeh, H. Saebfar, M.K. Mahabady, S. Orouei, K. Hushmandi, M. Entezari, M. Hashemi, A.R. Aref, M.R. Hamblin, H.L. Ang, A.P. Kumar, A. Zarrabi, S. Samarghandian, Overcoming doxorubicin resistance in cancer: siRNA-loaded nanoarchitectures for cancer gene therapy, Life Sci. 298 (2022) 120463.

[6] D. Cappetta, F. Rossi, E. Piegari, F. Quaini, L. Berrino, K. Urbanek, A. De Angelis, Doxorubicin targets multiple players: a new view of an old problem, Pharmacol. Res. 127 (2018).

[7] P.K. Singal, N. Iliskovic, Doxorubicin-induced cardiomyopathy, N. Engl. J. Med. 339 (1998) 900–905.

[8] D.S. Monahan, E. Flaherty, A. Hameed, G.P. Duffy, Resveratrol significantly improves cell survival in comparison to dexrazoxane and carvedilol in a h9c2 model of doxorubicin induced cardiotoxicity, Biomedicine & Pharmacotherapy = Biomedecine & Pharmacotherapie 140 (2021) 111702.

[9] S. Ravassa, A. Zudaire, J. Díez, GLP-1 and cardioprotection: from bench to bedside, Cardiovasc. Res. 94 (2012) 316–323.

[10] L.A. Nikolaidis, S. Mankad, G.G. Sokos, G. Miske, A. Shah, D. Elahi, R.P. Shannon, Effects of glucagon-like peptide-1 in patients with acute myocardial infarction and left ventricular dysfunction after successful reperfusion, Circulation 109 (2004) 962–965.

[11] G.G. Sokos, L.A. Nikolaidis, S. Mankad, D. Elahi, R.P. Shannon, Glucagon-like peptide-1 infusion improves left ventricular ejection fraction and functional status in patients with chronic heart failure, J. Card. Fail. 12 (2006) 694–699.

[12] J.A. Pan, H. Zhang, H. Lin, L. Gao, H.L. Zhang, J.F. Zhang, C.Q. Wang, J. Gu, Irisin ameliorates doxorubicin-induced cardiac perivascular fibrosis through inhibiting endothelial-to-mesenchymal transition by regulating ROS accumulation and autophagy disorder in endothelial cells, Redox Biol. 46 (2021) 102120.

[13] P. Qian, H. Tian, Y. Wang, W. Lu, Y. Li, T. Ma, X. Gao, W. Yao, A novel oral glucagon-like peptide 1 receptor agonist protects against diabetic cardiomyopathy via alleviating cardiac lipotoxicity induced mitochondria dysfunction, Biochem. Pharmacol. 182 (2020) 114209.

[14] G.A. Silberman, T.-H.M. Fan, H. Liu, Z. Jiao, H.D. Xiao, J.D. Lovelock, B. M. Boulden, J. Widder, S. Fredd, K.E. Bernstein, B.M. Wolska, S. Dikalov, D. G. Harrison, S.C. Dudley, Uncoupled cardiac nitric oxide synthase mediates diastolic dysfunction, Circulation 121 (2010) 519–528.

[15] L. Sun, Z. Meng, Y. Zhu, J. Lu, Z. Li, Q. Zhao, Y. Huang, L. Jiang, X. Yao, TM9SF4 is a novel factor promoting autophagic flux under amino acid starvation, Cell Death Differ. 25 (2018) 368–379.

[16] H. Lee, X. Jiang, I. Perwaiz, P. Yu, J. Wang, Y. Wang, M. Hüttemann, R.A. Felder, D.R. Sibley, B.M. Polster, S. Rozyyev, I. Armando, Z. Yang, P. Qu, P.A. Jose, Dopamine D5 receptor-mediated decreases in mitochondrial reactive oxygen species production are cAMP and autophagy dependent, Hypertens. Res. 44 (2021) 628–641.

[17] C. Zhang, H. Wang, X. Yang, Z. Fu, X. Ji, Y. Shi, J. Zhong, W. Hu, Y. Ye, Z. Wang, D. Ni, Oral zero-valent-molybdenum nanodots for inflammatory bowel disease therapy, Sci. Adv. 8 (2022) eabp9882.

[18] M.I. Love, W. Huber, S. Anders, Moderated estimation of fold change and dispersion for RNA-seq data with DESeq2, Genome Biol. 15 (2014) 550.

[19] J.G. Travers, S.A. Wennersten, B. Pena, R.A. Bagchi, H.E. Smith, R.A. Hirsch, L. A. Vanderlinden, Y.H. Lin, E. Dobrinskikh, K.M. Demos-Davies, M.A. Cavasin, L. Mestroni, C. Steinkuhler, C.Y. Lin, S.R. Houser, K.C. Woulfe, M.P.Y. Lam, T. A. McKinsey, HDAC inhibition reverses Preexisting diastolic dysfunction and blocks Covert extracellular matrix remodeling, Circulation 143 (2021) 1874–1890.

[20] G. Yu, L.-G. Wang, Y. Han, Q.-Y. He, clusterProfiler: an R package for comparing biological themes among gene clusters, OMICS 16 (2012) 284–287.

[21] L. Tian, L. Ma, E. Guo, X. Deng, S. Ma, Q. Xia, Y. Cao, S. Li, 20-Hydroxyecdysone upregulates Atg genes to induce autophagy in the Bombyx fat body, Autophagy 9 (2013) 1172–1187.

[22] A.H.M. Pereira, A.C. Cardoso, K.G. Franchini, Isolation, culture, and immunostaining of neonatal rat ventricular myocytes, STAR Protoc 2 (2021) 100950.

[23] X. Zhang, C. Hu, C.-Y. Kong, P. Song, H.-M. Wu, S.-C. Xu, Y.-P. Yuan, W. Deng, Z.-G. Ma, Q.-Z. Tang, FNDC5 alleviates oxidative stress and cardiomyocyte apoptosis in doxorubicin-induced cardiotoxicity via activating AKT, Cell Death Differ. 27 (2020) 540–555.

[24] O.J. Arola, A. Saraste, K. Pulkki, M. Kallajoki, M. Parvinen, L.M. Voipio-Pulkki, Acute doxorubicin cardiotoxicity involves cardiomyocyte apoptosis, Cancer Res. 60 (2000) 1789–1792.

[25] M. Yoshida, I. Shiojima, H. Ikeda, I. Komuro, Chronic doxorubicin cardiotoxicity is mediated by oxidative DNA damage-ATM-p53-apoptosis pathway and attenuated by pitavastatin through the inhibition of Rac1 activity, J. Mol. Cell. Cardiol. 47 (2009) 698–705.

[26] K. Min, O.-S. Kwon, A.J. Smuder, M.P. Wiggs, K.J. Sollanek, D.D. Christou, J.-K. Yoo, M.-H. Hwang, H.H. Szeto, A.N. Kavazis, S.K. Powers, Increased mitochondrial emission of reactive oxygen species and calpain activation are required for doxorubicin-induced cardiac and skeletal muscle myopathy, J. Physiol. 593 (2015) 2017–2036.

[27] K.M. Regula, K. Ens, L.A. Kirshenbaum, Inducible expression of BNIP3 provokes mitochondrial defects and hypoxia-mediated cell death of ventricular myocytes, Circ. Res. 91 (2002) 226–231.

[28] A. Dhingra, R. Jayas, P. Afshar, M. Guberman, G. Maddaford, J. Gerstein, B. Lieberman, H. Nepon, V. Margulets, R. Dhingra, L.A. Kirshenbaum, Ellagic acid antagonizes Bnip3-mediated mitochondrial injury and necrotic cell death of cardiac myocytes, Free Radic. Biol. Med. 112 (2017) 411–422.

[29] C. Cano, K. Saravanan, C. Bailey, J. Bardos, N.J. Curtin, M. Frigerio, B.T. Golding, I. R. Hardcastle, M.G. Hummersone, K.A. Menear, D.R. Newell, C.J. Richardson, K. Shea, G.C.M. Smith, P. Thommes, A. Ting, R.J. Griffin, 1-substituted (Dibenzo[b, d]thiophen-4-yl)-2-morpholino-4H-chromen-4-ones endowed with dual DNA-PK/PI3-K inhibitory activity, J. Med. Chem. 56 (2013) 6386–6401.

[30] A.C. Petropoulos, M. Moschovi, Cardiotoxicity among adult survivors suffered from childhood malignancies, Hellenic J. Nucl. Med. 22 (Suppl 2) (2019) 34–40.

[31] F.J.F. Broeyer, S. Osanto, J. Suzuki, F. de Jongh, H. van Slooten, B.C. Tanis, T. Bruning, J.J. Bax, H.J. Ritsema van Eck, M.L. de Kam, A.F. Cohen, Y. Mituzhima, J. Burggraaf, Evaluation of lecithinized human recombinant super oxide dismutase as cardioprotectant in anthracycline-treated breast cancer patients, Br. J. Clin. Pharmacol. 78 (2014) 950–960.

[32] D.K. Arulmozhi, B. Portha, GLP-1 based therapy for type 2 diabetes, Eur. J. Pharmaceut. Sci. 28 (2006).

[33] K.M. Heppner, D. Perez-Tilve, GLP-1 based therapeutics: simultaneously combating T2DM and obesity, Front. Neurosci. 9 (2015) 92.

[34] J. Lau, P. Bloch, L. Schäffer, I. Pettersson, J. Spetzler, J. Kofoed, K. Madsen, L. B. Knudsen, J. McGuire, D.B. Steensgaard, H.M. Strauss, D.X. Gram, S.M. Knudsen, F.S. Nielsen, P. Thygesen, S. Reedtz-Runge, T. Kruse, Discovery of the once-weekly glucagon-like peptide-1 (GLP-1) analogue semaglutide, J. Med. Chem. 58 (2015) 7370–7380.

[35] G. Tong, T. Peng, Y. Chen, L. Sha, H. Dai, Y. Xiang, Z. Zou, H. He, S. Wang, Effects of GLP-1 receptor agonists on biological behavior of colorectal cancer cells by regulating PI3K/AKT/mTOR signaling pathway, Front. Pharmacol. 13 (2022) 901559.

[36] C. Skriver, S. Friis, L.B. Knudsen, A.-M. Catarig, A.J. Clark, C. Dehlendorff, L. S. Mørch, Potential preventive properties of GLP-1 receptor agonists against prostate cancer: a nationwide cohort study, Diabetologia 66 (2023) 2007–2016.

[37] X. Lu, C. Xu, J. Dong, S. Zuo, H. Zhang, C. Jiang, J. Wu, J. Wei, Liraglutide activates nature killer cell-mediated antitumor responses by inhibiting IL-6/STAT3 signaling in hepatocellular carcinoma, Transl Oncol 14 (2021) 100872.

[38] A. Chequin, L.E. Costa, F.F. de Campos, A.D.B. Moncada, L.T.F. de Lima, L.R. Sledz, G.F. Picheth, E.R. Adami, A. Acco, M.B. Gonçalves, G.C.M. Manica, G. Valdameri, L. de Noronha, J.E.Q. Telles, E.H.F. Jandrey, E.T. Costa, F.F. Costa, E.M. de Souza, E.A.S. Ramos, G. Klassen, Antitumoral activity of liraglutide, a new DNMT inhibitor in breast cancer cells in vitro and in vivo, Chem. Biol. Interact. 349 (2021) 109641.

[39] F.S. Carvalho, A. Burgeiro, R. Garcia, A.J. Moreno, R.A. Carvalho, P.J. Oliveira, Doxorubicin-induced cardiotoxicity: from bioenergetic failure and cell death to cardiomyopathy, Med. Res. Rev. 34 (2014) 106–135.

[40] D. Chen, W. Yu, C. Zhong, Q. Hong, G. Huang, D. Que, Y. Wang, Y. Yang, B. Rui, Z. Zhuang, M. Liang, Z. Ye, X. Yan, J. Lv, R. Zhang, J. Yan, P. Yang, Elabela ameliorates doxorubicin-induced cardiotoxicity by promoting autophagic flux through TFEB pathway, Pharmacol. Res. 178 (2022) 106186.

[41] R. Dhingra, I. Rabinovich-Nikitin, S. Rothman, M. Guberman, H. Gang, V. Margulets, D.S. Jassal, K.N. Alagarsamy, S. Dhingra, C. Valenzuela Ripoll, F. Billia, A. Diwan, A. Javaheri, L.A. Kirshenbaum, Proteasomal degradation of TRAF2 mediates mitochondrial dysfunction in doxorubicin-cardiomyopathy, Circulation 146 (2022) 934–954.

[42] K. Hou, J. Shen, J. Yan, C. Zhai, J. Zhang, J.-A. Pan, Y. Zhang, Y. Jiang, Y. Wang, R. Z. Lin, H. Cong, S. Gao, W.-X. Zong, Loss of TRIM21 alleviates cardiotoxicity by suppressing ferroptosis induced by the chemotherapeutic agent doxorubicin, EBioMedicine 69 (2021) 103456.

[43] C.-Y. Kong, Z. Guo, P. Song, X. Zhang, Y.-P. Yuan, T. Teng, L. Yan, Q.-Z. Tang, Underlying the mechanisms of doxorubicin-induced acute cardiotoxicity: oxidative stress and cell death, Int. J. Biol. Sci. 18 (2022) 760–770.

[44] D.A. Kubli, M.N. Quinsay, C. Huang, Y. Lee, A.B. Gustafsson, Bnip3 functions as a mitochondrial sensor of oxidative stress during myocardial ischemia and reperfusion, Am. J. Physiol. Heart Circ. Physiol. 295 (2008) H2025–H2031.

[45] D.A. Kubli, J.E. Ycaza, A.B. Gustafsson, Bnip3 mediates mitochondrial dysfunction and cell death through Bax and Bak, Biochem. J. 405 (2007) 407–415.

[46] R. Dhingra, V. Margulets, S.R. Chowdhury, J. Thliveris, D. Jassal, P. Fernyhough, G.W. Dorn, L.A. Kirshenbaum, Bnip3 mediates doxorubicin-induced cardiac myocyte necrosis and mortality through changes in mitochondrial signaling, Proc. Natl. Acad. Sci. U.S.A. 111 (2014) E5537–E5544.

[47] M. Iwasa, H. Kobayashi, S. Yasuda, I. Kawamura, S. Sumi, Y. Yamada, T. Shiraki, T. Yamaki, H. Ushikoshi, T. Aoyama, K. Nishigaki, G. Takemura, T. Fujiwara, H. Fujiwara, S. Minatoguchi, Antidiabetic drug voglibose is protective against ischemia-reperfusion injury through glucagon-like peptide 1 receptors and the

phosphoinositide 3-kinase-Akt-endothelial nitric oxide synthase pathway in rabbits, J. Cardiovasc. Pharmacol. 55 (2010) 625–634.

[48] O. Erdogdu, D. Nathanson, A. Sjöholm, T. Nyström, Q. Zhang, Exendin-4 stimulates proliferation of human coronary artery endothelial cells through eNOS-, PKA- and PI3K/Akt-dependent pathways and requires GLP-1 receptor, Mol. Cell. Endocrinol. 325 (2010) 26–35.

[49] E. Favaro, R. Granata, I. Miceli, A. Baragli, F. Settanni, P. Cavallo Perin, E. Ghigo, G. Camussi, M.M. Zanone, The ghrelin gene products and exendin-4 promote survival of human pancreatic islet endothelial cells in hyperglycaemic conditions, through phosphoinositide 3-kinase/Akt, extracellular signal-related kinase (ERK) 1/2 and cAMP/protein kinase A (PKA) signalling pathways, Diabetologia 55 (2012) 1058–1070.